Experimental section

Text S1

Materials and Chemicals: Hemp leaves were harvested from the hemp experimental field in Qiqihar (Heilongjiang Province, China) which was utilized as the feedstocks for the preparation of CQDs. Zinc nitrate ($Zn(NO_3)_2{\cdot}6H_2O$), iron nitrate ($Fe(NO_3)_2{\cdot}9H_2O$), L-Ascorbic acid (L-AA) and ammonium fluoride (NH_4F) were purchased from Tianjin Kaifang Chemical Reagent Co., Ltd. Ethanol (C_2H_5OH) and potassium iodide (KI) were purchased from Tianjin Tianli Chemical Reagent Co., Ltd. Melamine ($C_3H_6N_6$) was obtained from Beijing Inokai Technology Co., Ltd. Cyanuric acid ($C_3H_3N_3O_3$), levofloxacin (LFX), benzoquinone (p-BQ), isopropanol (IPA), L-Histidine (L-his), methanol (MeOH) and nitroblue tetrazolium (NBT) are provided by Shanghai Macklin Biochemical Technology Co., Ltd. Terephthalic acid (TA) is provided by Shanghai yuanye Bio-Technology Co., Ltd. The deionized water was applied for the preparation of the reactive solution.

Text S2

Material characterization: The morphology and elementary composition of the prepared samples were analyzed by scanning electron microscopy (SEM) coupled with energy dispersive spectrometer (EDS) (Hitachi, S-4300, Japan) and transmission electron microscopy (TEM) (Hitachi, H-7650, Japan). X-ray diffraction (XRD) measurements were performed on X-ray diffractometer using Cu Kα radiation as X-ray source which was operated at 60 kV and 80 mA (Bruker, AXS(D8), German). X-ray photoelectron spectra (XPS) of the samples were recorded on a X-ray photoelectron spectrometer (VG, EscaLab 250Xi, Britain) with Al Kα X-ray radiation at 300 W. The Fourier transform infrared spectra (FT-IR) were gained using a Fourier transform infrared spectrophotometer (PE Company, America) with a resolution of 2 cm^{-1} and a wavenumber range from 400 to 4000 cm^{-1} using KBr discs. UV-visible diffuse reflectance spectroscopy (DRS) was performed to characterize the light absorption property and determine the absorption edge wavelength of the synthesized samples. The photoluminescence (PL) spectra of samples were recorded on a Hitachi F4600 spectrophotometer under the excitation on wavelength of 325 and 365 nm. The specific surface area and corresponding pore structure of the samples were determined by N_2 absorption-desorption isotherms measurement in the static volumetric absorption analyzer (Micromeritics, ASAP 2020, America). The Brunauer-Emmett-Teller (BET) adsorption formula and Barrett-Joyner-Halenda (BJH) analysis method were applied for the calculation on the specific surface area values and the pore distribution curves of the samples. The reactive oxygen species (ROS) during the degradation process were investigated by electron spin resonance (ESR) spectroscopy on a Bruker EMX Plus spectrometer at 9.44 GHz at 300 K.

Text S3

Electrochemical measurement: The photoelectrochemical properties of the synthesized photocatalysts were characterized on a standard three-electrodes system in an electrochemical workstation (Chenhua 660E, China), in which the catalyst coated F-doped SnO_2 (FTO) glass, Ag/AgCl electrode, Pt sheet were used as the working electrode, reference electrode and counter electrode and 0.1 mol/L Na_2SO_4 solution was employed as the electrolyte. With Nafion solution (0.2 mL) as electrolyte, FTO glass as, as and as, photocurrent response was measured in three electrode cells. Especially, the catalyst coated FTO electrode were prepared accord to the following steps: Use the following typical procedure to prepare the photoelectrode. Firstly, a catalyst ink was prepared by dispersing 20 mg the as-prepared catalyst into 1 mL of a mixture of 5% Nafion solution and ethanol (v:v, 1:9) under energetical ultrasound treatment for 30 min. Then, the working electrode was constructed by coating the catalyst ink onto a cleaned FTO glass with an active area of 1 cm^2 using drop coating method (1×2 cm^2). Using the above three electrode system, the instantaneous photocurrent response (I-t) was collected using an on-off cycle model under xenon lamp irradiation with light intensity of 200 W (PLS-FX300HU, China). Electrochemical impedance (EIS) was investigated at a frequency range of 10^{-2}–10^5 Hz under an alternating voltage of 10 mV. The Mott-Schottky curve was measured at a voltage of 10 mV and an amplitude frequency of 1 K Hz. The Cyclic voltammetry (CV) tests were performed at varied scan rates in a non-Faradic region.

Thereby, the double-layer specific capacitance (C_{dl}) values of catalysts were gained by calculating the slope of the linear relationship between capacitive currents vs scan rates [2]. The electrochemical surface area (ECSA) of the catalysts were estimated by the following:

$$ECSA = C_{dl} / C_s$$

where C_{dl} refers to the above-derived double layer capacitance and C_s is the specific capacitance of a planar surface under the same electrolyte condition. Generally, the C_s represents the specific capacitance of ideal plate electrode with a constant value of 0.04 μF/cm^2 in 0.1 mol/L Na_2SO_4.

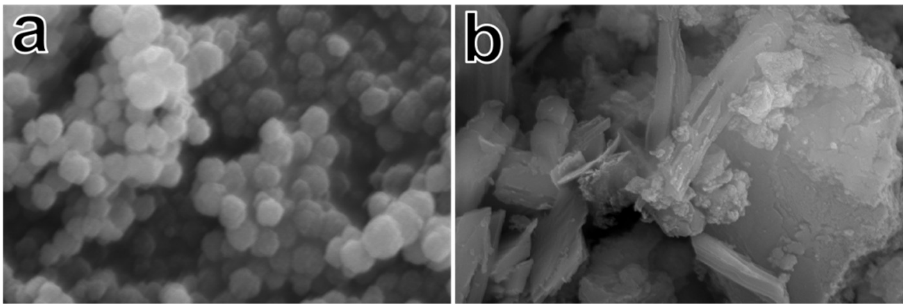

Figure S1 SEM images of (a) $ZnFe_2O_4$, (b) bluk g-C_3N_4

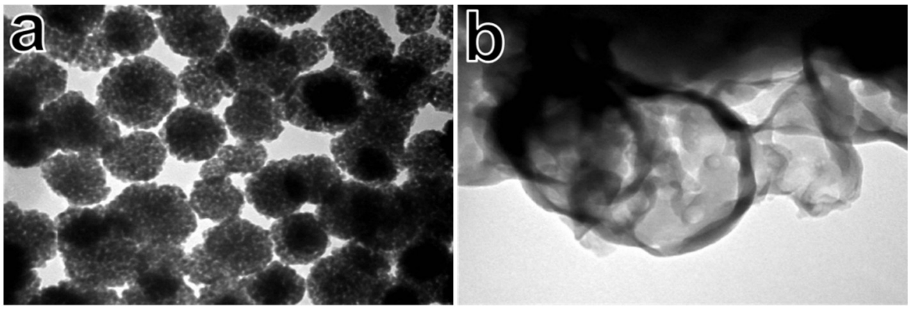

Figure S2 TEM images of (a) $ZnFe_2O_4$, (b) CNC-0.01

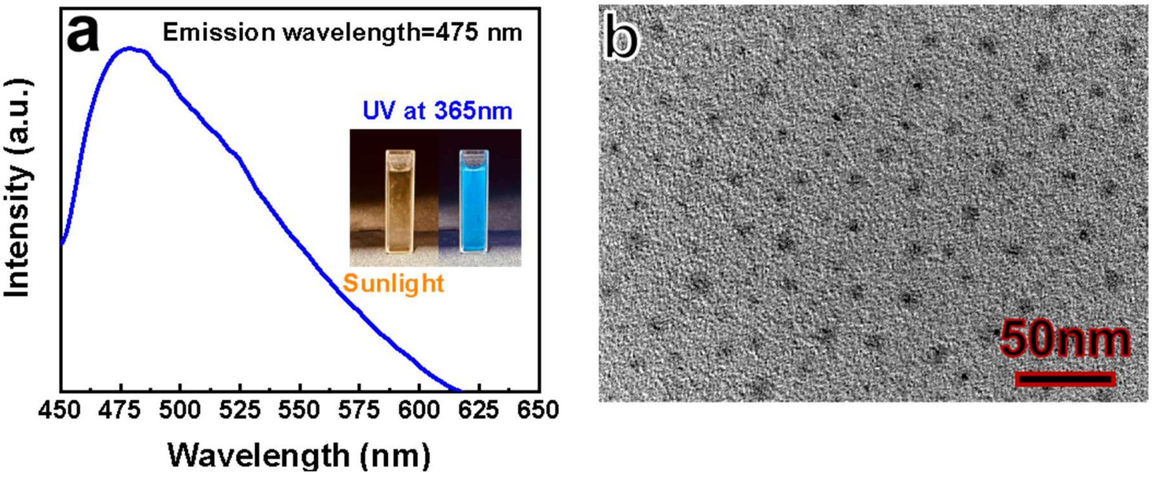

Figure S3 (a) PL spectrum, (b) TEM image.of CQDs. Inset of Figure S3a: Photographs of the as-prepared N,F-CQDs solution under sunlight (left) and UV light at 365 nm (right)

Table S1 The specific surface area and pore structure parameters of as-prepared samples

Photocatalyst	Surface area/($m^2 \cdot g^{-1}$)	Mean pore diameter/nm	Total pore volume/($cm^3 \cdot g^{-1}$)
$ZnFe_2O_4$	25.272	3.421	0.1941
g-C_3N_4	14.366	23.095	0.0256
CNC	70.226	18.154	0.0907
ZCC	56.379	5.623	0.1141

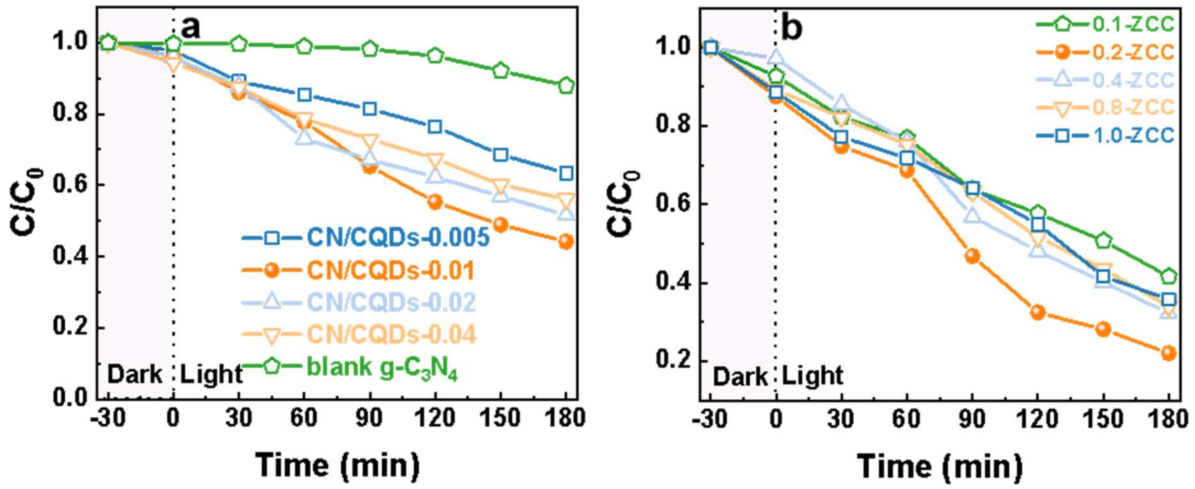

Figure S4 (a) Optimization of addition amount of CQDs and (b) $ZnFe_2O_4$ in ZCC

Table S2 Comparison of LFX degradation of different nanocomposites under visible light irradiation

Catalyst	Dosage/mg	Concentration/(mgs·L^{-1})	Removal rate/%	Ref.
ZCC	20	20	95.3	This study
Sm_6WO_{12}/g-C_3N_4	50	10	90.8	[3]
g-C_3N_4/Bi_2WO_6	20	10	85.8	[4]
Ag_2O/P-g-C_3N_4	50	10	83	[5]
g-C_3N_4/$Ti_3C_2T_X$/Ag_3PO_4	60	10	80.73	[6]
BiOI/$BiVO_4$/g-C_3N_4	50	20	89.01	[7]

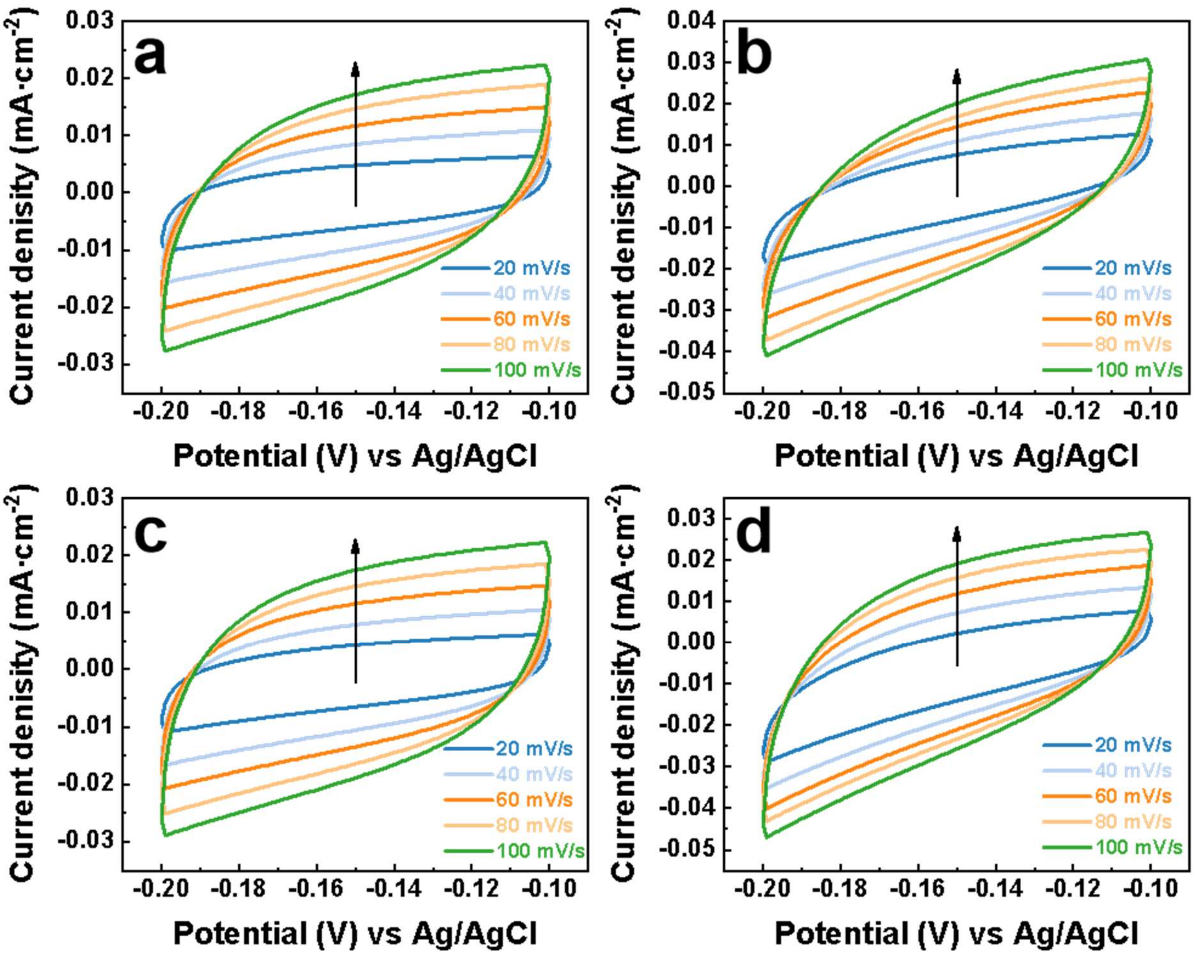

Figure S5 CV curves with different rates from 20 to 100 mV/s for (a) g-C_3N_4, (b) $ZnFe_2O_4$, (c) CNC and (d) 0.2-ZCC in 0.1 M Na_2SO_4

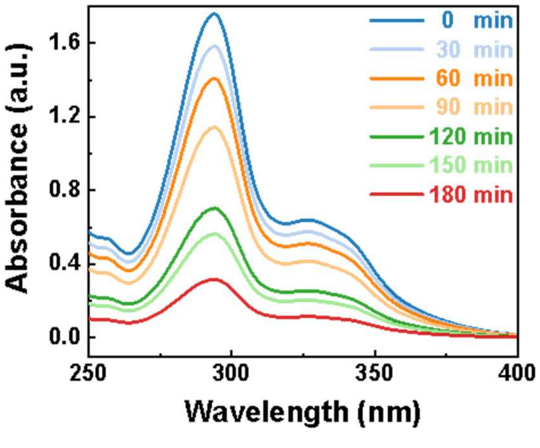

Figure S6 UV-vis spectra of LFX degradation during the first cycle degradation

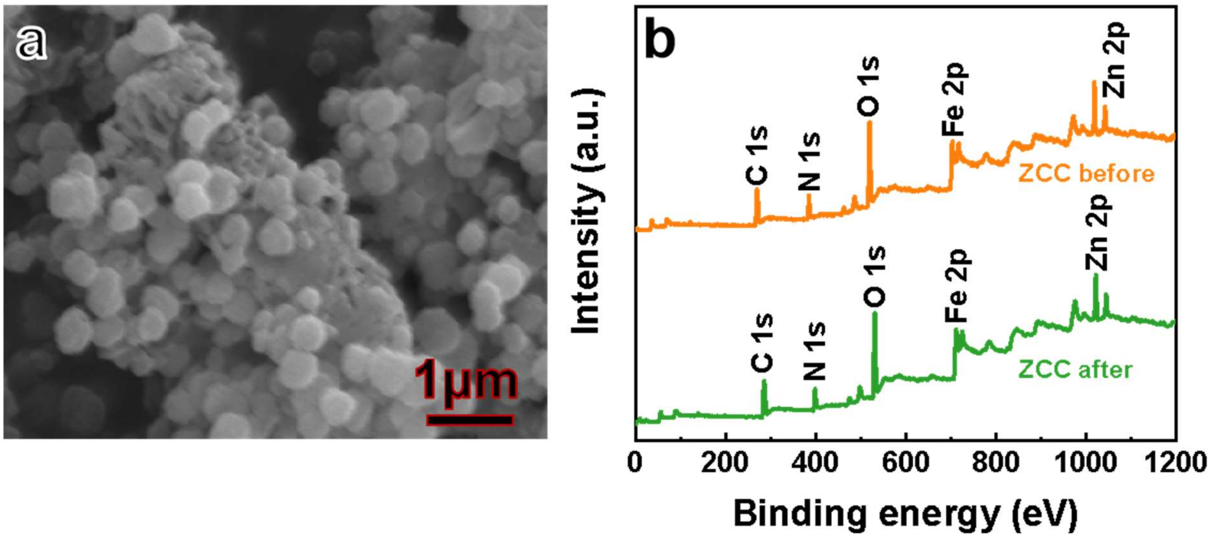

Figure S7 (a) SEM image of the used ZCC composite and (b) XPS spectra of the fresh and used ZCC photocatalyst

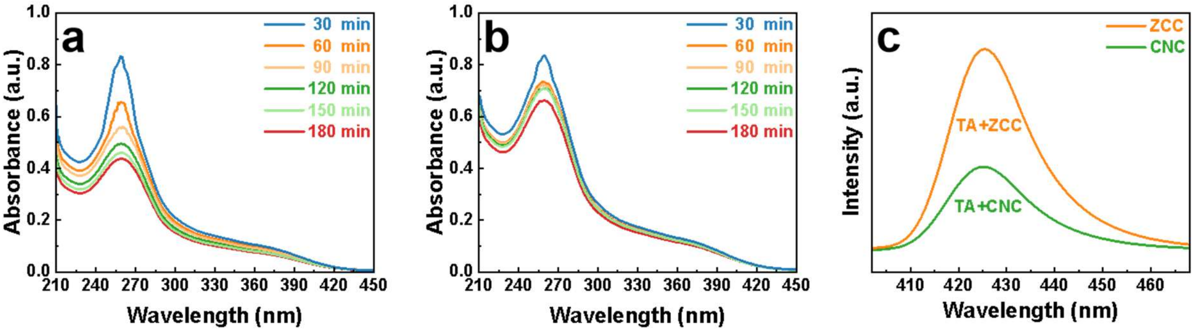

Figure S8 UV-vis absorption spectra of the NBT solution reacted with (A) CNC and (B) ZCC, (C) PL spectra of terephthalic acid (TA) reacted with ZCC and CNC

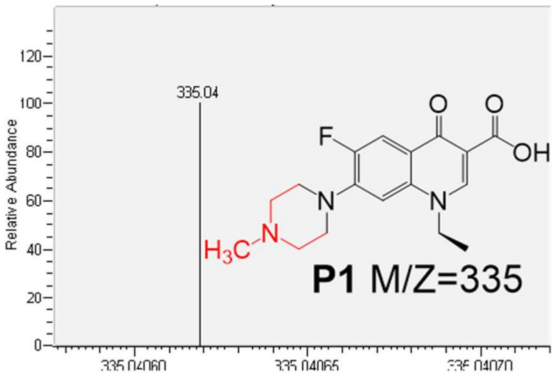
Relative Abundance
0
20
40
60
80
100
120
335.04
335.04060
335.04065
335.04070
F
O
O
OH
N
N
N
H_3C
P1 M/Z=335

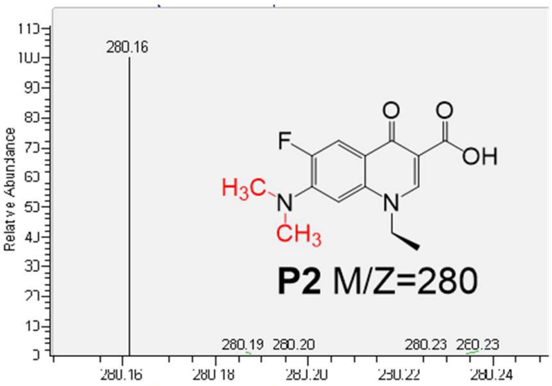
Relative Abundance
0
10
20
30
40
50
60
70
80
90
100
110
280.16
280.19
280.20
280.23
280.23
280.16
280.18
280.20
280.22
280.24
F
O
O
OH
H_3C
N
CH_3
N
P2 M/Z=280

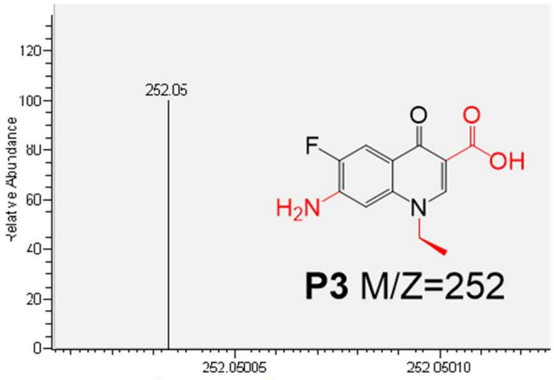
Relative Abundance
0
20
40
60
80
100
120
252.05
252.05005
252.05010
F
O
O
OH
H_2N
N
P3 M/Z=252

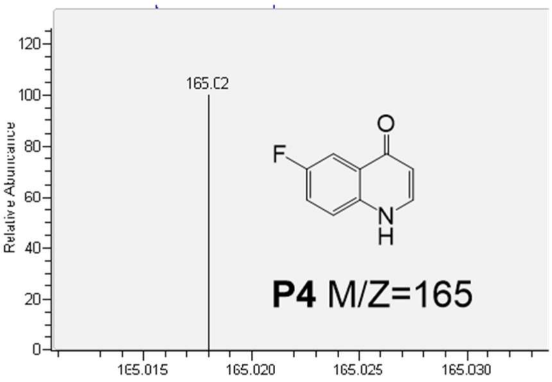
Relative Abundance
0
20
40
60
80
100
120
165.02
165.015
165.020
165.025
165.030
F
O
N
H
P4 M/Z=165

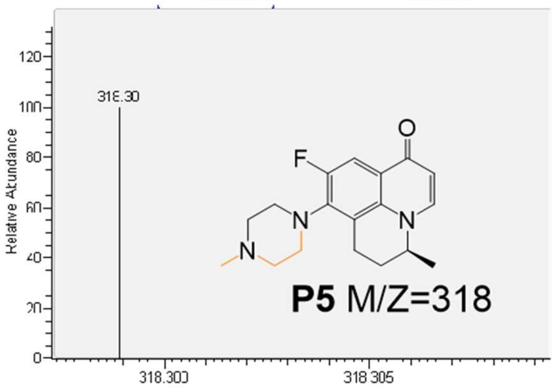
Relative Abundance
0
20
40
60
80
100
120
318.30
318.300
318.305
F
O
N
N
N
P5 M/Z=318

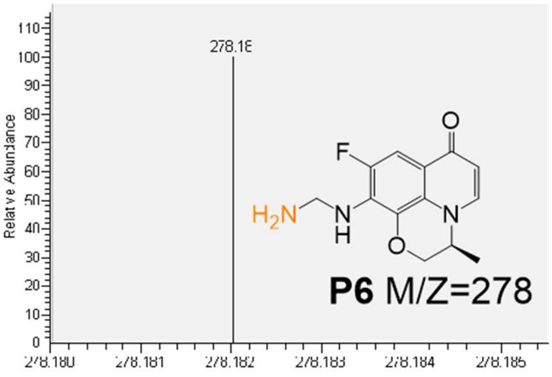
Relative Abundance
0
10
20
30
40
50
60
70
80
90
100
110
278.18
278.180
278.181
278.182
278.183
278.184
278.185
F
O
H_2N
N
H
N
O
P6 M/Z=278

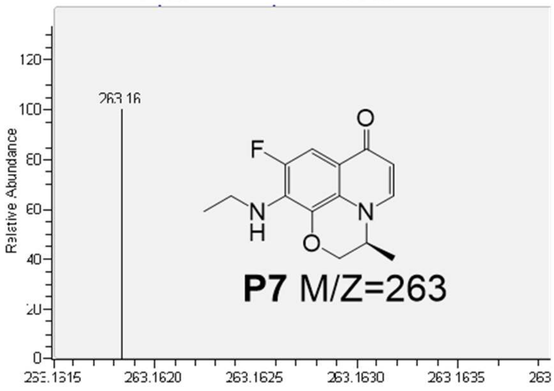
Relative Abundance
0
20
40
60
80
100
120
263.16
263.1615
263.1620
263.1625
263.1630
263.1635
263
F
O
N
H
N
O
P7 M/Z=263

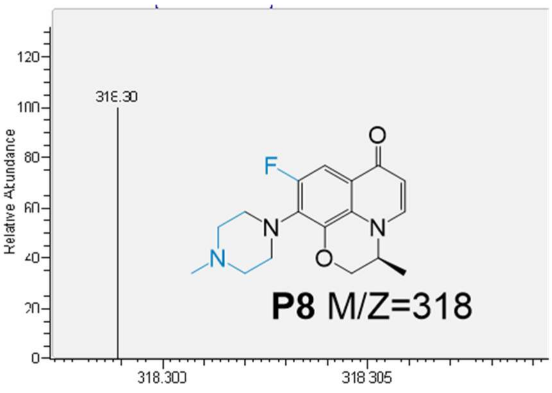
Relative Abundance
0
20
40
60
80
100
120
318.30
318.300
318.305
F
O
N
N
N
O
P8 M/Z=318

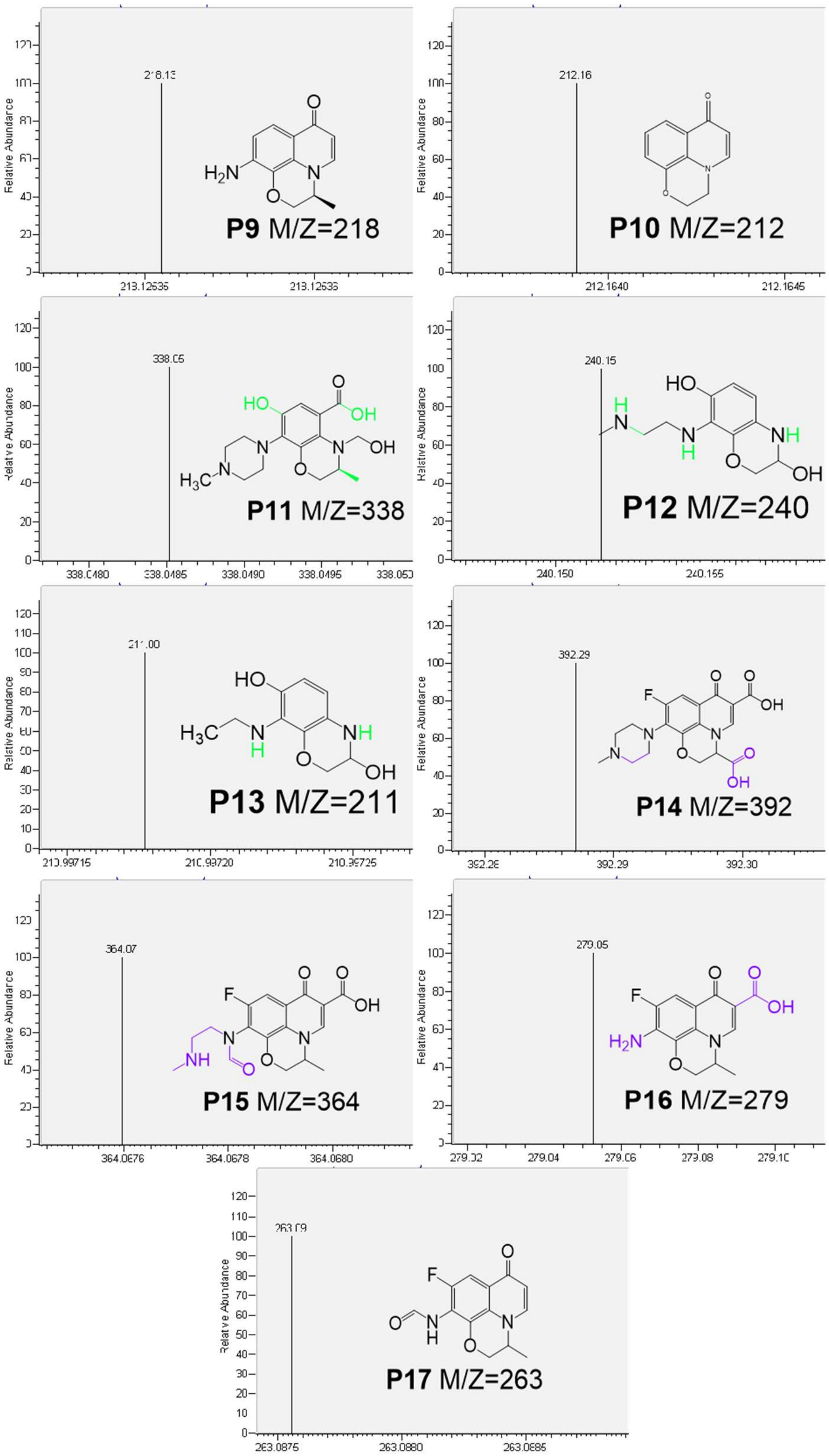

Figure S9 Mass spectra graphs of the identified intermediates during the levofloxacin degradation

Table S3 The identified possible intermediate products during levofloxacin degradation from the LC-MS data

Name	Empirical formula	Molecular structure	m/z value/(g·mol^{-1})
LFX	$C_{18}H_{20}FN_3O_4$	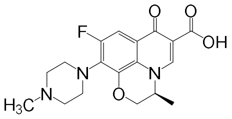	361
P1	$C_{17}H_{20}FN_3O_3$	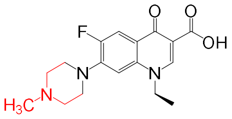	335
P2	$C_{14}H_{15}FN_2O_3$	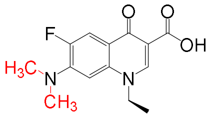	280
P3	$C_{12}H_{11}FN_2O_3$	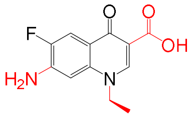	252
P4	C_9H_6FNO	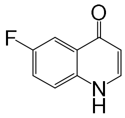	165
P5	$C_{18}H_{22}FN_3O$	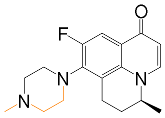	318
P6	$C_{13}H_{14}FN_3O_2$	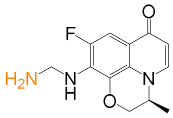	278
P7	$C_{14}H_{15}FN_2O_2$	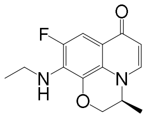	263
P8	$C_{17}H_{20}FN_3O_2$	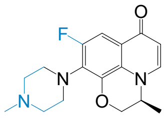	318
P9	$C_{12}H_{12}N_2O_2$	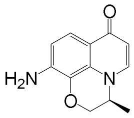	218
P10	$C_{11}H_9NO_2$	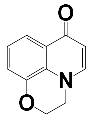	212
P11	$C_{16}H_{23}N_3O_5$	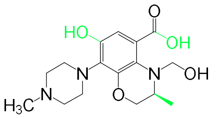	338
P12	$C_{11}H_{17}N_3O_3$	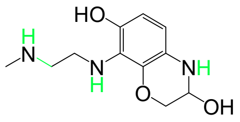	240
P13	$C_{10}H_{14}N_2O_3$	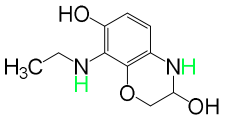	211

P14	$C_{18}H_{18}FN_3O_6$	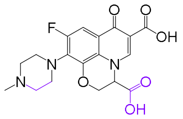	392
P15	$C_{17}H_{18}FN_3O_5$	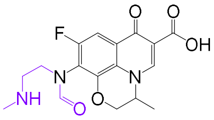	364
P16	$C_{13}H_{11}FN_2O_4$	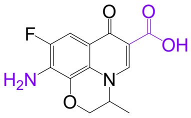	279
P17	$C_{13}H_{11}FN_2O_3$	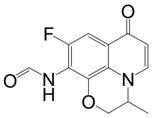	263

References

[1] DONG Guo-hua, CHI Wei-meng, CHAI Dong-feng, et al. A novel Ag_3BiO_3/ZnO/BC composite with abundant defects and utilizing hemp BC as charge transfer mediator for photocatalytic degradation of levofloxacin [J]. Applied Surface Science, 2023, 619: 156732. DOI: 10.1016/j.apsusc.2023.156732.

[2] PRABAVATHI S L, SARAVANAKUMAR K, PARK C M, et al. Photocatalytic degradation of levofloxacin by a novel Sm_6WO_{12}/g-C_3N_4 heterojunction: Performance, mechanism and degradation pathways [J]. Separation and Purification Technology, 2021, 257: 117985. DOI: 10.1016/j.seppur.2020.117985.

[3] MA Bing-rui, ZHA Yu-xin, YU Peng, et al. Hydrothermal nanoarchitectonics of Z-scheme g-C_3N_4/Bi_2WO_6 heterojunction with enhanced adsorption and photocatalytic activity for fluoroquinolone antibiotics removal: Kinetics, mechanism and degradation pathway [J]. Journal of Alloys and Compounds, 2023, 952: 170061. DOI: 10.1016/j.jallcom.2023.170061.

[4] ZHANG Xin-fei, ZHANG Yuan, WANG Zi-wei, et al. Construction of a novel Ag_2O/P-g-C_3N_4 p-n type heterojunction for efficient degradation of organic pollutants under visible light irradiation [J]. Diamond and Related Materials, 2022, 130: 109398. DOI: 10.1016/j.diamond.2022.109398.

[5] LIAO Dan, XU Jia-jie, LIU Chang-kun. Constructing MXene-derived Z-Scheme g-C_3N_4/Ti3C2TX/Ag_3PO_4 photocatalysts with enhanced charge transfer for aquatic organic pollutants removal [J]. Colloids and Surfaces A: Physicochemical and Engineering Aspects, 2023, 675: 132050. DOI: 10.1016/j.colsurfa.2023.132050.

[6] ZHU Peng-fei, LUO Dan, LIU Mei, et al. Flower-globular BiOI/BiVO4/g-C_3N_4 with a dual Z-scheme heterojunction for highly efficient degradation of antibiotics under visible light [J]. Separation and Purification Technology, 2022, 297: 121503. DOI: 10.1016/j.seppur.2022.121503.